MICRO-SEISMIC EVALUATION OF FRACTURING IN CORES DURING TRIAXIAL COMPRESSION TESTS

Y. Xiao, A. Abugharara and S.D. Butt
Advanced Drilling Laboratory, Memorial University of Newfoundland, St. John's, NL, Canada

This paper was prepared for presentation at the International Symposium of the Society of Core Analysts held in St. John's Newfoundland and Labrador, Canada, 16-21 August, 2015

ABSTRACT

This study is an evaluation of rock cracking and failure by means of laboratory standard strength tests and real time micro-seismic or acoustic emission (AE) monitoring. Three groups of rock-like materials were cast using fine aggregate and Portland cement, out of which standard test specimens were cored. Confined compression strength (CCS) tests were conducted on those cores while two non-destructive testing (NDT) sensors were placed in end platens used to compress the core. Conventional rock mechanics results were obtained such as stress-strain response. Hundreds of micro-seismic events were recorded in the process of rock deformation and especially when the core failed. Seismic data processing indicated the synchronization of event occurrence rate with correlated material deformation. Also, micro-seismic properties were analyzed such as dominant frequency (DF), event energy and cumulative AE counts. Event energy was found closely related to the peak amplitude of seismic waves. Under the same confining pressure, DF was prone to decrease with increase of deformation until the core failed. This correlated with the higher AE event rate when deformation increased. High strength material tended to generate higher DF than that of low strength material. For the same strength material, increasing confining pressure played different roles on the dominant frequency. Finally, AE event occurrence locations were determined along the core length which was compared with the observation of core surface cracks.

INTRODUCTION

Micro-seismic events or AE are the elastic waves produced when rock undergoes internal change, such as micro-crack initiation and propagation. Piezoelectric transducers are commonly employed in detecting and monitoring micro-crack propagation [1]. As an alternative way to 'see' micro-crack initiation and propagation, AE detection was applied in triaxial compression tests to monitor the whole deformation process [2]. Some AE parameters such as DF, event energy and cumulative AE counts are related to the different deformation stages [3, 4]. Source location was conducted to identify the approximate location of AE events applied in hydraulic fracturing researches [5, 6, 7]. Numerical simulation was used to simulate the deformation process and predict the failure [8, 9]. Crack type was also classified based on detected acoustic emissions for failure prediction [10, 11, 12, 13].

EXPERIMENTAL SETUP

Monitoring AE during the CCS test was scheduled. The CCS tests were conducted using a servo-controlled axial loading frame and a Hoek triaxial pressure cell. AE were recorded using a two-sensor AE system.

Axial Loading Frame

During the CCS test, axial load was applied by the Instron load frame (Figure 1). The maximum loading could be 250 kN. By setting the loading rate of 1 mm/min, extension and load were recorded until the core specimen failed. The core was put into the Hoek triaxial cell and specific confining pressure was loaded by a manually operated pump.

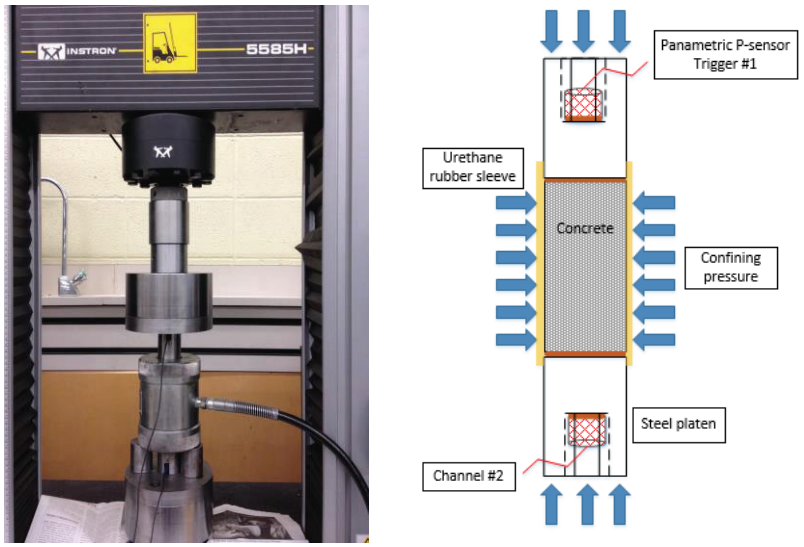

Figure 1. Strength test apparatus with the Hoek triaxial cell (left) and working schematic (right).

Monitoring Acoustic Emission

Two Panametrics p-wave sensors were placed into steel platens on both ends of core specimens (Figure 1). Sponge material was put between the sensors and the loading frame for complete contact assurance and p-wave couplant was put between the steel platens and core ends and between sensors and steel platens to make better signal transmittal. The central frequency of the p-wave sensors was 1.14 MHz with working bandwidth of from 0.65 to 1.63 MHz at -6dB attenuation. Two PAC 2/4/6 preamplifiers were utilized and gain selection of 40dB. Two customized power supply adapters were connected to the preamplifiers with output voltage of 20 volt. The DAQ system was comprised of GaGe CompuScope 8280 eight-channel board and its included DAQ software. The trigger sensor was always located on the top of cores. Inputs for AE detection are listed in Table 1.

Table 1. Inputs for monitoring acoustic emission.

Sampling frequency	P-wave sensors #	Gain	Peak-peak input	Trigger level
10 MHz	2	40 dB	10 V	0.15 V

Test Materials

Three groups of rock-like materials were used with UCS (0 confining pressure) at 20, 55.5 and 87.5 MPa, designated as low, medium and high strengths (L, M and H) in Figure 2. These materials were made of fine aggregate, Portland cement and water. This type of rock-like materials has been used in all previous lab tests in this project based on the ability of the reproducibility. Such tests were performed to study the drill-ability including AE. In this paper, AE tests were conducted to investigate the deformation and cracking properties which were valuable for future bit-rock interaction investigation, but petroleum cores were not involved. Standard NQ cores were drilled with core diameter of 47.6 mm and the minimum ratio of height to diameter was 2:1. All the coring process and requirements were done in accordance to ASTM D4543 [14]. Averaged core dimensions and the loading plan are given in Table 2. To be consistent with the investigation of rock-like material's properties and mechanical response, confining pressures were chosen in accordance to previous rock characterization tests.

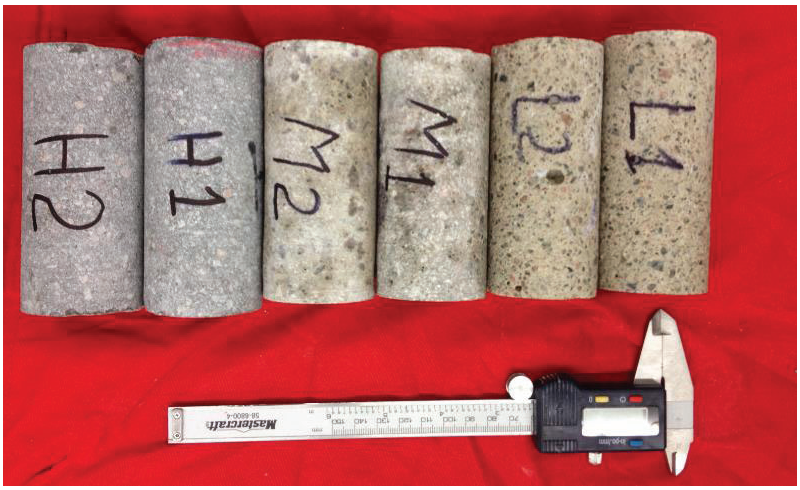

Figure 2. Tested concrete cores (low, medium and high strength).

Table 2. Loading plan for triaxial compression test and CCS results.

Core #	Length (mm)	Diameter (mm)	P-wave velocity (m/s)	Conf. Pres. (MPa)	CCS (MPa)
L1	111.64	47.23	4304.0	2	33.90
L2	105.04	47.22	4304.0	4	41.48
M1	100.79	47.38	4785.4	2	59.84
M2	103.47	47.18	4785.4	4	75.36
H1	108.39	47.43	4710.4	2	105.65
H2	104.88	47.51	4710.4	4	116.11

Overall Workflow

The overall flow chart for this test is shown in Figure 3. Acoustic emission signals from cracking were automatically detected and saved to the AE computer disk. At the same

time, CCS test was being conducted and the stress and strain data were recorded into the other computer. Both the computers were synchronized before each test began.

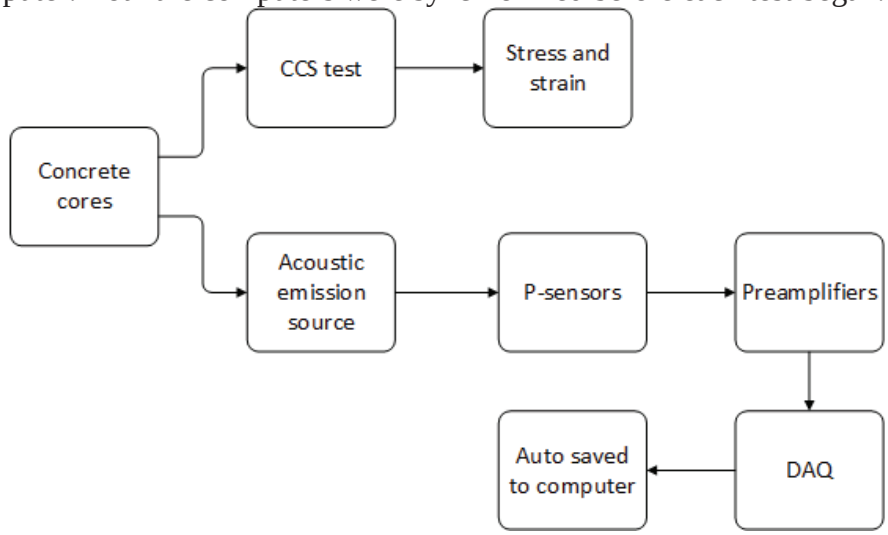

Figure 3. Flow chart of CCS test with monitoring acoustic emissions.

RESULTS

The CCS tests [15] were conducted with the results in Table 2 and acoustic responses were also obtained. Analysis of events includes DF, event energy, peak amplitude, cumulative AE number and event location interpretation from the relative travel time was numerically processed.

Single Acoustic Emission

A single event from a CCS test was obtained in Figure 4. The top sensor was always set as the trigger channel and two bursts of signals were captured at both sensors. The different first arrival time demonstrated that the AE source located closer to the top sensor. AE parameters were calculated based on methodology previously developed [3].

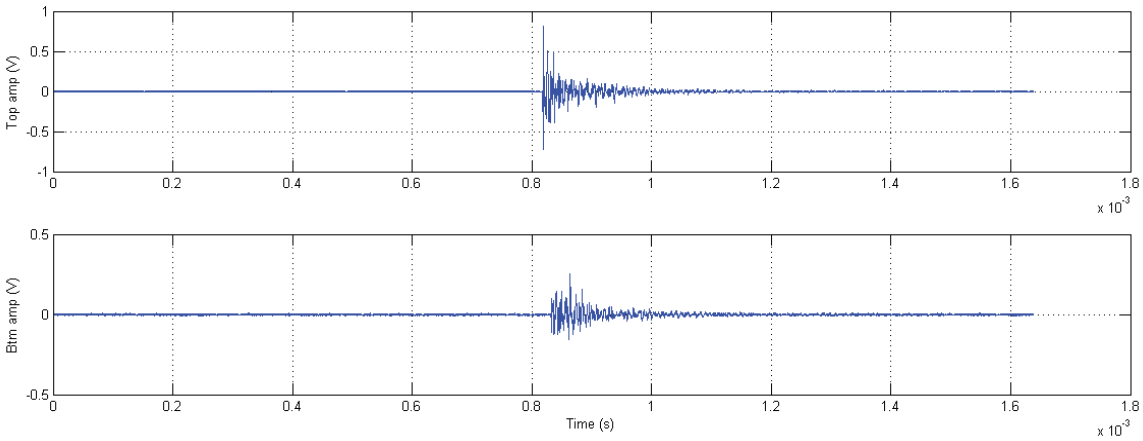

Figure 4. One burst event from top sensor (upper) and bottom sensor (lower) detected from the high strength material with 4 MPa confining pressure.

Single Test Inspection

AE event locations were determined and only those from inside the cores were kept. The mechanical response and acoustic properties of low, medium and high strength cores were plotted together for comparison in Figure 5-7. Stress and cumulative AE counts were plotted on the same time base. Before the linear loading section, few AE events were detected. AE events initiated at the end of the linear loading sections and the number increased within non-linear ductile deformation section. This was explained by the initiation of micro-cracks and micro-crack connection. AE rate dramatically increased before and after the core failed. This was due to the micro-crack propagation and crack nucleation that was continuously generated.

Event energy and peak amplitude were also investigated from both sensors. Event energy was found closely correlated with peak amplitude. And energy from both sensors correlated with each other. This indicated that a single channel of signals could be used for AE analysis.

For medium strength cores, limited AE events were detected due to less capability of signal transmittal between core surfaces and sensors.

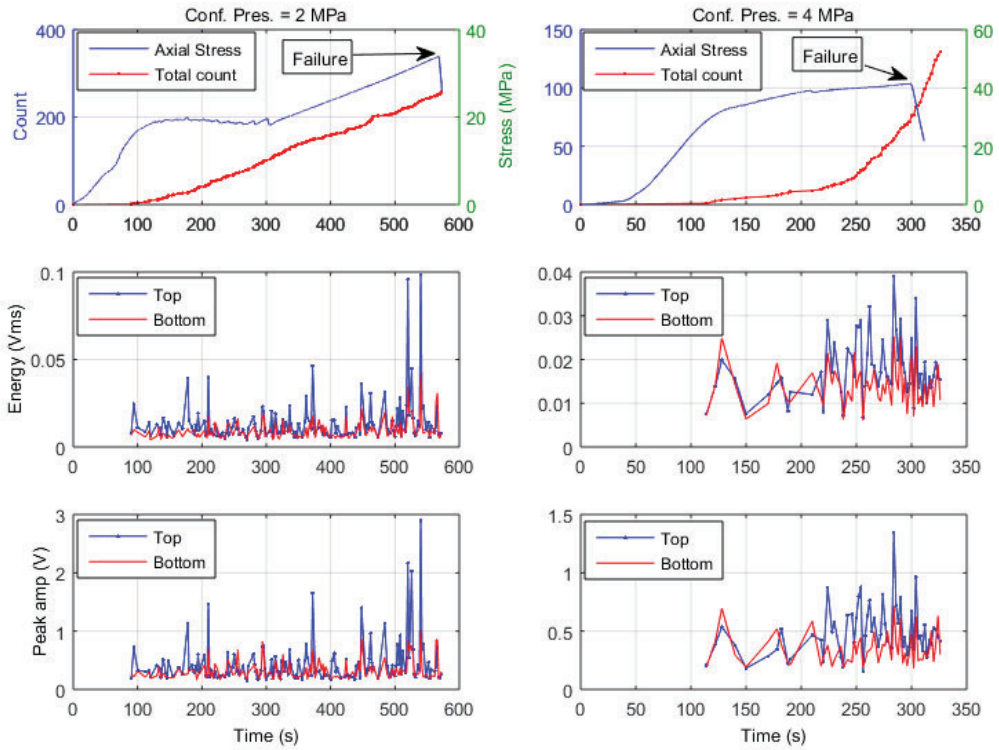

Figure 5. Mechanical and acoustic responses of low strength cores with acoustic properties comparison from both sensors.

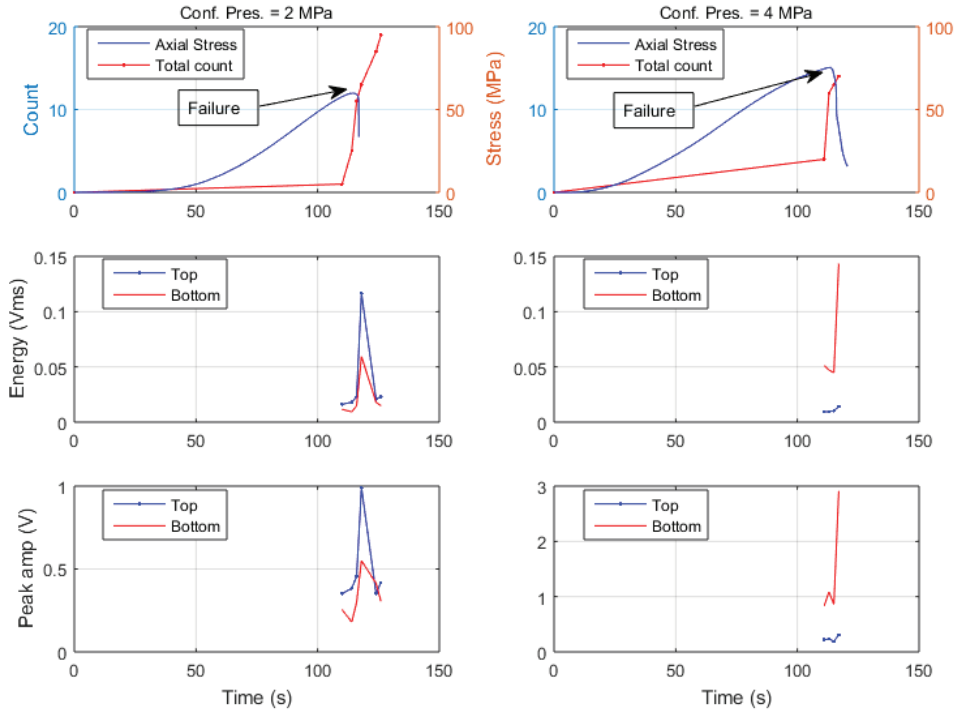

Figure 6. Mechanical and acoustic responses of medium strength cores with acoustic properties comparison from both sensors.

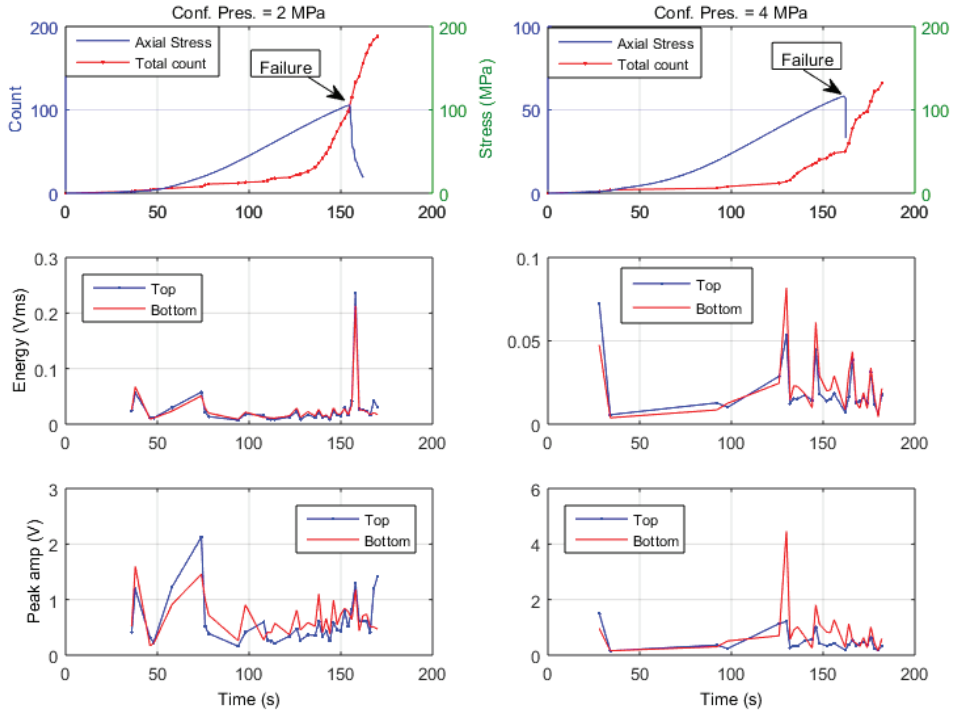

Figure 7. Mechanical and acoustic responses of high strength cores with acoustic properties comparison from both sensors.

Dominant Frequency and Source Energy

DF and AE event energy of signals from the top trigger sensor were compared for all tests in Figure 8 and Figure 9, separately. Linear fit was plotted for each group of scattered points to the test time. Under the same confining pressure, DF tends to decrease with the increase of core deformation. For the low strength material, DF stays constant during the rock deformation process. There is no evidence to show the relation of material strength and the DF level.

AE event energy generally decreases with increased DF under the same confining pressure. An exception exists that event energy increases with increased DF for the medium strength material under the confining pressure of 2 MPa.

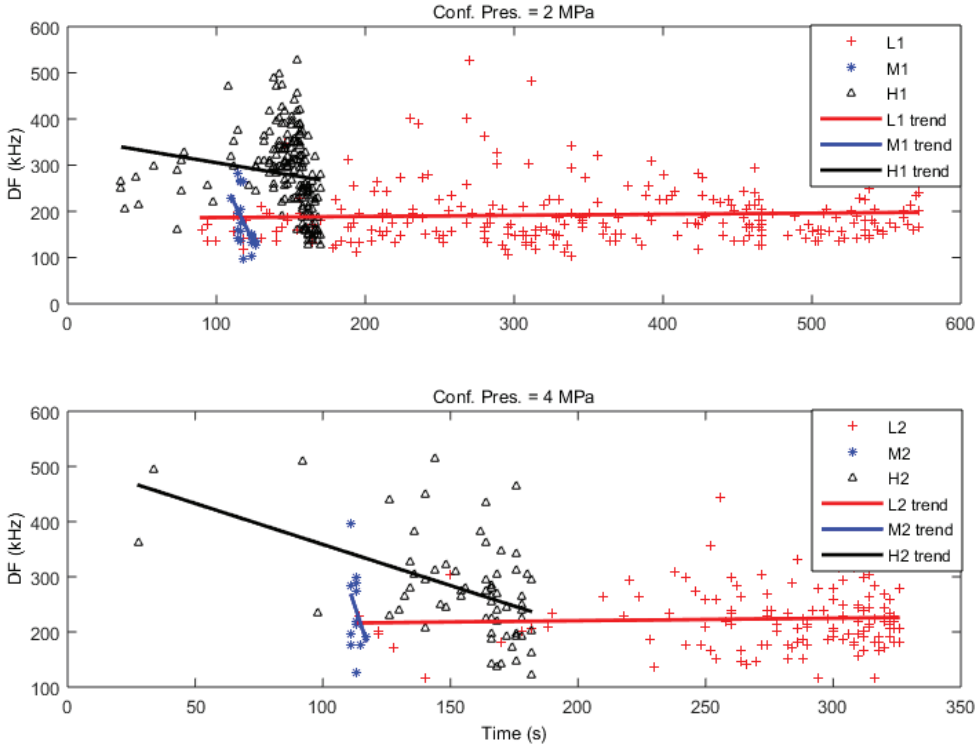

Figure 8. DF versus time for low, medium and high strength cores under confining pressure of 2 MPa (upper) and 4 MPa (lower). Linear fit was provided for each group of scattered points.

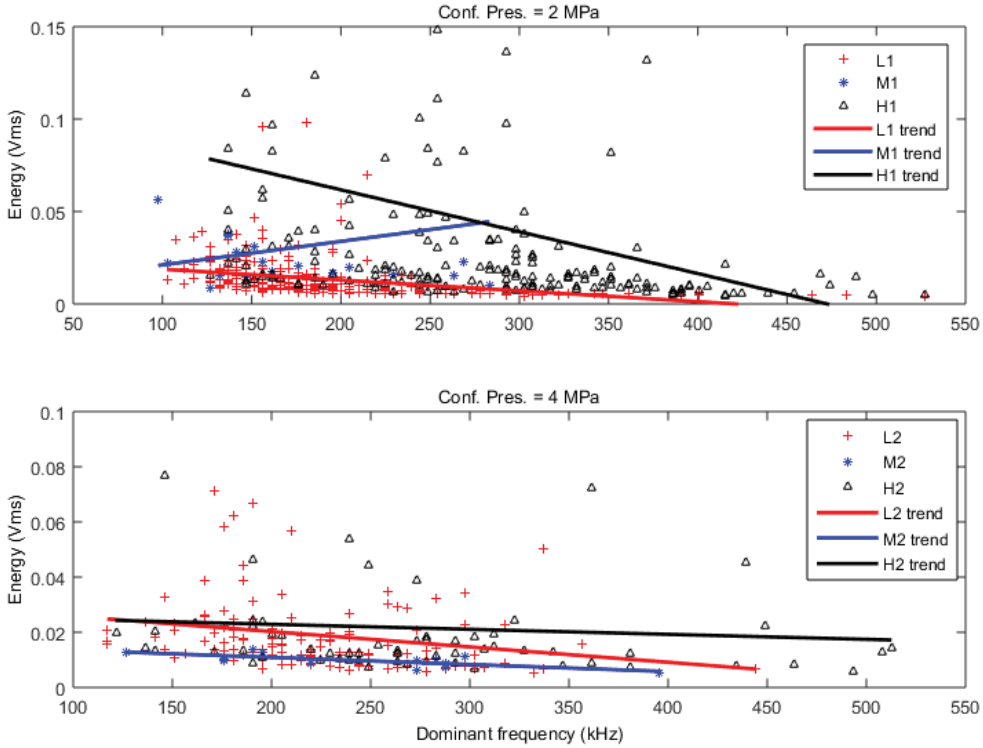

Figure 9. AE energy versus dominant frequency for low, medium and high strength cores under confining pressure of 2 MPa (upper) and 4 MPa (lower). Linear fit was provided for each group of scattered points.

Source Location and Failure Observation

The AE source location was obtained and plotted versus the test time in Figure 10. The vertical axes are scaled to the actual core lengths. For low strength material, the majority of AE events were located in the upper half of the core under both confining pressures. This coincides with the observed results. For medium strength material, there was limited number of AE sources due to lack of good sensor contact. For high strength material, AE sources were distributed more uniformly along the length of the core.

The above AE distribution characteristics or cracks were observed from the post failure demonstration in Figure 11. The cores failed due to shear cracking and macroscopic cracks propagate along all the length of the cores. Cracks mainly distributed along one portion of core length for low strength material, which was possibly due to unevenly distributed axial stress.

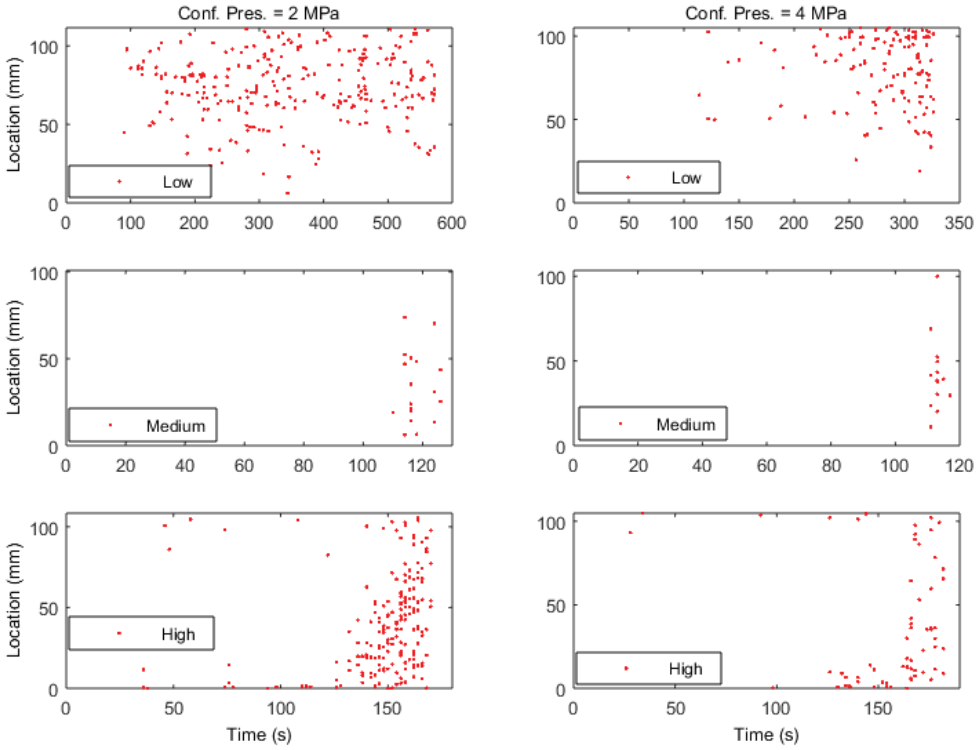

Figure 10. One dimensional acoustic source distribution versus test time for low, medium and high strength cores. Vertical axes were scaled to actual core heights.

CONCLUSIONS

AE provides one feasible technique of characterizing rock deformation and failure in the laboratory. AE event rates correlate with the rock failure.

AE event DF tends to decrease with increased deformation. Also, event energy tends to decrease with increased dominant frequency. There is no evident relationship between DF and CCS.

AE source location was plotted versus time along the length of the cores. For low strength cores, AE sources were mainly distributed on one end which was observed in the failed specimens. For medium strength and high strength cores, AE sources were more uniformly distributed along the core length.

Figure 11. Post failure illustration for low, medium and high strength cores under confining pressure of 2 MPa.

ACKNOWLEDGEMENTS

The project is funded by Atlantic Canada Opportunity Agency, Husky Energy, Suncor Energy and Research and Development Corporation (RDC) of Newfoundland and Labrador under AIF contract number: 781-2636-1920044.

REFERENCES

1. Hardy, H.R. Jr., "Applications of Acoustic Emission Techniques to Rock and Rock Structures: A State-of-the-Art Review", *Acoustic Emissions in Geotechnical Engineering Practice, American Society for Testing and Materials*, (1981), 4-92.
2. Lockner, D., "The role of acoustic emission in the study of rock fracture", *Int. J. Rock Mech. Min. Sci. & Geomech. Abstr*., (1993) **30**, 7, 883-899.
3. Butt, S.D. and P.N. Calder, "Experimental Procedure to Measure Volumetric Changes and Microseismic Activity During Triaxial Compression Tests", *Int. J. Rock Mech. Min. Sci.*, (1998) **35**, 2, 249-254.
4. Keshavarz, M., F.L. Pellet and K.A. Hosseini, "Comparing the effectiveness of energy and hit rate parameters of acoustic emission for prediction of rock failure",

in *ISRM International Symposium on Rock Mechanics,* 2009, The University of Hong Kong, China.
5. Damani, A., A. Sharma, C.H. Sondergeld and C.S. Rai, "Mapping of Hydraulic Fractures under Triaxial Stress Conditions in Laboratory Experiments using Acoustic Emissions", In *SPE Annual Technical Conference and Exhibition*, 2012, San Antonio, Texas.
6. Chitrala, Y., C.H. Sondergeld and C.S. Rai, "Microseismic Studies of Hydraulic Fracture Evolution at Different Pumping Rates", in *SPE Americas Unconventional Resources Conference*, 2012, Pittsburgh, Pennsylvania.
7. Fortin, J., S. Stanchits, G. Dresen and Y. Gueguen. "Acoustic Emissions Monitoring during Inelastic Deformation of Porous Sandstone: Comparison of Three Modes of Deformation", *Pure and Applied Geophysics*, (2009).
8. Cai, M., P.K. Kaiser, Y. Tasaka, H. Kurose, M. Minami and T. Maejima, "Numerical Simulation of Acoustic Emission in Large-scale Underground Excavations", in *The 42nd US Rock Mechanics Symposium*, 2008, San Francisco, CA.
9. Tang, C., P.K. Kaiser and G. Yang. "Numerical Simulation of Seismicity In Rock Failure", *2nd North American Rock Mechanics Symposium*, 1996, 19-21 June, Montreal, Quebec, Canada.
10. Zang, A., C. Wagner, F., S. Stanchits, G. Dresen, R. Andresen, and M.A. Haidekker. "Source analysis of acoustic emissions in Aue granite cores under symmetric and asymmetric compressive loads", *Geophysical Journal*, (1998) **135**, 3, 1113-1130.
11. Aggelis, D.G. "Classification of cracking mode in concrete by acoustic emission parameters", *Mechanics Research Communications*, (2011) **38**, 3, 153–157.
12. Ohno, K. and M. Ohtsu. "Crack classification in concrete based on acoustic emission", *Construction and Building Materials*, (2010) **24**, 12, 2339–2346.
13. Chow, T.M. "Concurrent ultrasonic tomography and acoustic emission in solid materials", Doctoral dissertation, Queen's University at Kingston, 1992.
14. ASTM D4543-08, *Standard Practices for Preparing Rock Core as Cylindrical Test Specimens and Verifying Conformance to Dimensional and Shape Tolerances*, ASTM International, West Conshohocken, PA, 2008, www.astm.org.
15. ASTM D7012-14, *Standard Test Methods for Compressive Strength and Elastic Moduli of Intact Rock Core Specimens under Varying States of Stress and Temperatures*, ASTM International, West Conshohocken, PA, 2014, www.astm.org.